Nanoscale

PAPER

View Article Online
View Journal | View Issue

Cite this: *Nanoscale*, 2015, **7**, 14889

Chelator free gallium-68 radiolabelling of silica coated iron oxide nanorods *via* surface interactions†

Benjamin P. Burke,[a,b] Neazar Baghdadi,[a] Alicja E. Kownacka,[a] Shubhanchi Nigam,[a,b] Gonçalo S. Clemente,[b,c] Mustafa M. Al-Yassiry,[a] Juozas Domarkas,[a,b] Mark Lorch,[a] Martin Pickles,[d] Peter Gibbs,[d] Raphaël Tripier,[e] Christopher Cawthorne[b,c] and Stephen J. Archibald*[a,b]

Received 28th April 2015,
Accepted 6th August 2015

DOI: 10.1039/c5nr02753e

www.rsc.org/nanoscale

The commercial availability of combined magnetic resonance imaging (MRI)/positron emission tomography (PET) scanners for clinical use has increased demand for easily prepared agents which offer signal or contrast in both modalities. Herein we describe a new class of silica coated iron–oxide nanorods (NRs) coated with polyethylene glycol (PEG) and/or a tetraazamacrocyclic chelator (DO3A). Studies of the coated NRs validate their composition and confirm their properties as *in vivo* T_2 MRI contrast agents. Radiolabelling studies with the positron emitting radioisotope gallium-68 ($t_{1/2}$ = 68 min) demonstrate that, in the presence of the silica coating, the macrocyclic chelator was not required for preparation of highly stable radiometal-NR constructs. *In vivo* PET-CT and MR imaging studies show the expected high liver uptake of gallium-68 radiolabelled nanorods with no significant release of gallium-68 metal ions, validating our innovation to provide a novel simple method for labelling of iron oxide NRs with a radiometal in the absence of a chelating unit that can be used for high sensitivity liver imaging.

1. Introduction

Medical imaging can be defined as the non-invasive visualisation of the intact human body for clinical analysis. Positron Emission Tomography (PET) is a nuclear medicine technique based on the detection of positron emitting radionuclides to give a high sensitivity functional image.[1–3] However, as a molecular imaging technique, it does not provide anatomical information and is, therefore, often combined with other techniques, such as computed tomography (CT) or magnetic resonance imaging (MRI). Although the combination of PET with CT is most prevalent in the clinic, recent developments in detector design have led to the creation of combined PET/MR scanners that offer advantages over PET/CT, such as increased soft tissue contrast, lower radiation dose and the potential application of MRI contrast agents.[4,5] The introduction of clinical PET/MRI scanners increases the demand for multimodal contrast agents, achieved either by using a cocktail of known imaging agents or by developing new dual modality contrast agents in which both components are linked into one construct.[6–9]

Super-paramagnetic iron oxide nanoparticles (SPIONs) are used in MRI to reduce the time taken for proton nuclei to transfer their spin to neighbouring proton nuclei, resulting in a loss of transverse magnetisation (T_2 relaxation), causing a relative darkening in regions of SPION accumulation.[10,11] Iron–oxide based nanospheres have been the most commonly used T_2 contrast agents clinically,[12–14] largely because of their low toxicity and the potential for facile modification of the surface.[15–17] Iron–oxide based nanorods (NRs) are less common but may offer advantages, such as improved MRI contrast[18–20] and improved properties as drug delivery vehicles.[21]

^{68}Ga ($t_{1/2}$ = 68 min) is an attractive radioisotope for PET due to high proportion of positron decay (89%) and its availability from a generator based system as a decay product of a parent isotope with a long half-life (^{68}Ge, $t_{1/2}$ = 271 days), eliminating the need for an onsite cyclotron.[22,23] In aqueous solution and

[a]*Department of Chemistry, University of Hull, Cottingham Road, Hull, HU6 7RX, UK. E-mail: s.j.archibald@hull.ac.uk*
[b]*Positron Emission Tomography Research Centre, University of Hull, Cottingham Road, Hull, HU6 7RX, UK*
[c]*School of Biological, Biomedical and Environmental Sciences, University of Hull, Cottingham Road, Hull, HU6 7RX, UK*
[d]*Centre for Magnetic Resonance Investigations, Hull York Medical School at University of Hull, Anlaby Road, Hull, HU3 2JZ, UK*
[e]*Université de Brest, UMR-CNRS 6521/SFR148 ScInBioS, UFR Sciences et Techniques, 6 Avenue Victor le Gorgeu, C.S. 93837, 29238 Brest, France*
†Electronic supplementary information (ESI) available. See DOI: 10.1039/c5nr02753e

at physiological pH, ^{68}Ga is exclusively in the oxidation state +3, thus most synthetic procedures are carried out in the presence of weakly coordinating ligands such as citrate, acetate or oxalate at low pH in order to avoid the formation of insoluble $Ga(OH)_3$ and soluble $Ga(OH)_4^-$, both of which dramatically slow the kinetics of complex formation.[24,25] Gallium(III) generally forms six coordinate complexes and is classified as a hard Lewis acid, therefore, it binds to borderline and hard Lewis base donor atoms such as nitrogen and oxygen, found in routinely used chelators for biomedical imaging.[26,27] Incorporation of ^{68}Ga into a targeting vector is generally achieved by the use of bifunctional chelating agents (BCAs), molecules containing a chelating moiety responsible for trapping ^{68}Ga in a stable *in vivo* form, functionalised with a reactive group allowing its conjugation to a bioactive molecule, protein or peptide.[28,29] 1,4,7,10-Tetraazacyclododecane-1,4,7,10-tetraacetic acid (DOTA) is the most widely employed BCA due to the relative ease of its synthesis (due to its chemical symmetry) and the ability to complex, with adequate stability, various metal ions relevant for a range of biomedical applications.[3,22,30,31]

Herein we describe the development of silica coated iron oxide NRs radiolabelled with gallium-68 for PET/MR multimodal imaging in which the inclusion of a bifunctional chelating agent (such as DOTA) is not required for stable gallium(III) complexation *in vivo*.

2 Results & discussion

2.1. Synthesis and surface characterisation

Iron–oxide nanorods, coated with various ratios of a siloxane terminated tetraazamacrocycle (siloxane-DO3A) and a siloxane polyethylene glycol (PEG) derivative, were synthesised using a modified method, similar to that previously reported by our group.[32] Briefly, uncoated iron oxide nanorods and the selected ratio of functionalised siloxanes were stirred in a basic 60% ethanol/water solution, as shown in Scheme 1. The preparation includes a rigorous washing procedure followed by resuspension of coated NRs in water and removal of macro aggregates by filtration through a 0.45 μm filter. Macrocycle coated nanoparticles were subsequently subjected to trifluoroacetic acid (TFA) hydrolysis to unmask the protected acetate arms to give nanoparticles coated using 100% macrocycle (**1**) and 50% macrocycle, 50% PEG (**2**). The 100% PEG coated NRs (**3**) do not require a hydrolysis step.

Transmission electron microscopy (TEM) analysis was carried out on the final constructs (**1–3**) to ensure that synthetic coating protocols do not affect the core iron–oxide structure, see Fig. 1. All constructs were found to have a similar size distribution, with rods of length 80–130 nm. Fourier transform infra-red (FTIR) spectroscopy was carried out to validate the presence of the surface coating, see Fig. 2. All coating types had the expected stretches of Fe–O, Si–O–C and Si–O–Fe between 600 and 1000 cm^{-1}.[33] Surface coatings can be differentiated due to the independent peak characteristics of each type. In case of **1**, characteristic macrocycle-derived C–N stretches can be assigned at *ca.* 1200 cm^{-1}. In case of **3**, C–O–C linkage, characteristic to PEG, can be assigned at 1117 cm^{-1}. **2** was designed to contain a mixture of coating component and was produced using a 1 : 1 ratio of the two coating components, with the FTIR showing a broad peak in the region overlapping both regions. The chemical composition of surface coating is corroborated by combustion analysis of coated NRs nitrogen content (0.79, 0.29 and 0.00% for **1**, **2** and **3**, respectively) as the only inclusion of nitrogen is from the

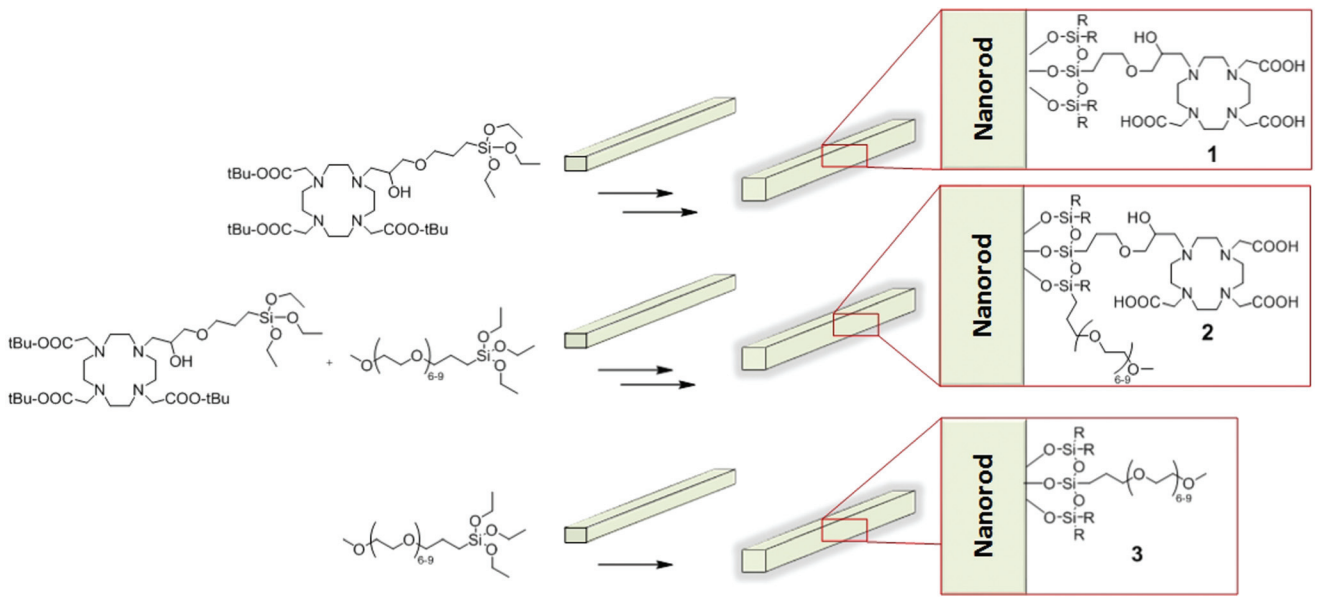

Scheme 1 Synthesis of silica coated iron oxide nanorods **1–3**.

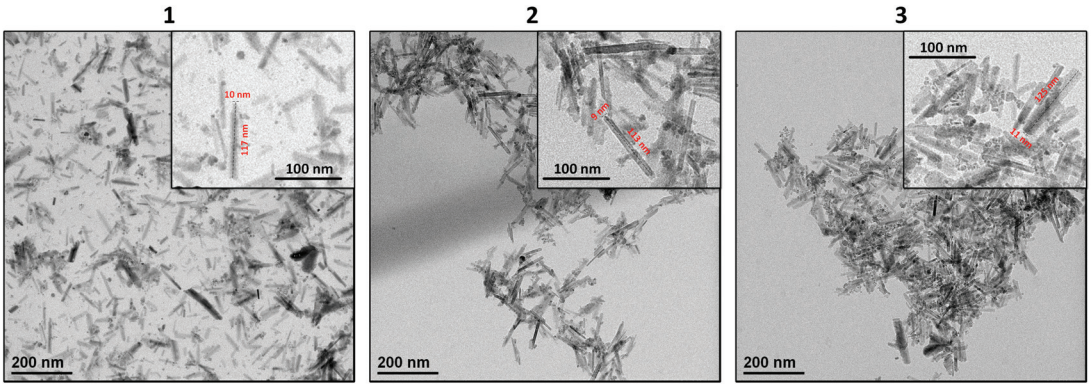

Fig. 1 TEM images of iron oxide nanorods **1–3**.

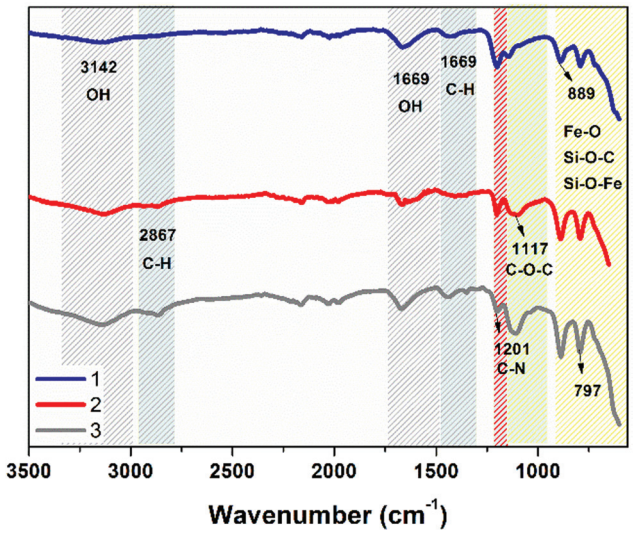

Fig. 2 FTIR spectra of nanorods **1–3**.

tetraazamacrocycle coating, decreasing for **2** relative to **1** as expected, see Fig. S1.†

2.2. Nanorod construct analysis

The surface charge of nanoparticles gives an indication of their aqueous suspension stability, an essential requirement for translation to *in vivo* studies. A large negative or positive value would suggest an increased electrostatic repulsion between individual nanoparticles, decreasing the tendency for aggregation.[34–36] The zeta potential of the constructs (**1–3**) was measured at a constant concentration (7.5 mM Fe) at pH 7 in PBS, see Fig. S2.† All constructs have an overall negative charge between −10 and −20 mV. Analogous PEG methyl ether terminating nanoparticles have a similar surface charge[37] and DOTA based systems have deprotonated carboxylic acid groups at pH 7.[38,39] All constructs have a relatively similar zeta potential, with **2** having the highest negative potential at −17.9 mV. The high negative surface charge of all constructs translates to high stability in aqueous solution, with no visible precipitation observed for any of the samples after 2 months.

The size of nanoparticles is an important characteristic governing their *in vivo* biodistribution pathways and, therefore, determining their potential for application as MRI contrast agents. Very small (<5 nm) nanoparticles are generally eliminated *via* the renal system and large (>200 nm) nanoparticles are excreted *via* the spleen and liver. Either of these elimination pathways results in short blood circulation times.[10,40,41] Samples of all three constructs were suspended in water (at a concentration of 0.1 mM Fe) and their hydrodynamic size was measured by nanoparticle tracking analysis (NTA) in which mean and modal sizes were determined, see Fig. S3.† The constructs had mean sizes in the range of 99–155 nm, with an increase in size correlating with the addition of macrocycle to the surface coating, all are an acceptable size for *in vivo* applications. There are challenges with NTA analysis and the use of rods rather than spheres: (a) how do these numbers relate to the different nanorod axes?; and (b) are the *in vivo* excretion pathways of the nanorods different to that of the nanospheres and, if so, what is the effect of length?

Prior to radiolabelling and *in vivo* studies, the magnetic behaviour of the NR constructs was investigated *in vitro* at 3 T, a magnetic field strength correlating to common clinical MRI scanners. The r_1 and r_2 relaxation rates were calculated for all three constructs (**1–3**), see Fig. 3 and 4. All constructs are relatively weak T_1 contrast agents. As T_2 contrast agents, all constructs showed fast relaxivity with improvement correlated to the increasing PEG content of the NR coating.

The large variability in both r_1 and r_2 values, as a function of chemical composition of surface coating, could be explained by a combination of factors, such as variation of hydrodynamic size, hydrophilicity and permeability of the different coatings to water molecules.[42] The increase in hydrodynamic size inversely correlates with both r_1 and r_2 values. Although superparamagnetic contrast agents generate a long-range magnetic field for the spin-spin relaxation (T_2) process, this effect decreases as distance increases. Similarly, as the mechanism for transverse (T_1) relaxation is proximity based, an increase in coating thickness leads to a decrease in r_1

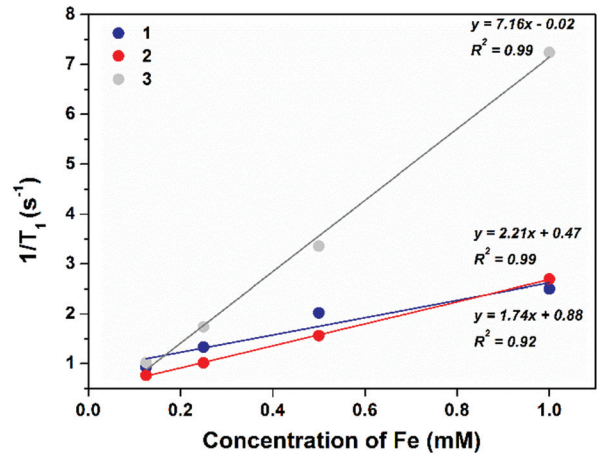

Fig. 3 T_1 MRI relaxivity plots of **1–3** at a range of Fe concentrations (0.1–1 mM) at 3 T to determine r_1.

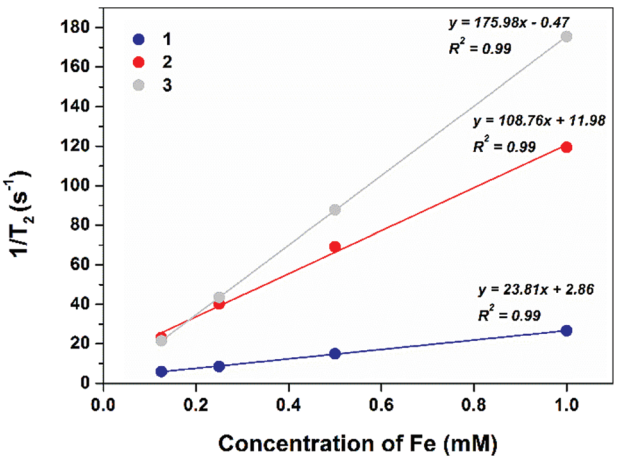

Fig. 4 T_2 MRI relaxivity plots of **1–3** at a range of Fe concentrations (0.1–1 mM) at 3 T to determine r_2.

values.[43] The hydrophilicity and permeability of the surface coating also has an effect on relaxivity rates,[44] although more relevant for T_1 relaxation, varying the ease of water molecule access to the iron surface. The more easily that water molecules can transfer into close proximity with the iron surface, and exchange rapidly, the faster the relaxivity rates.

2.3. Gallium-68 radiolabelling and stability

In aqueous solutions, gallium is almost exclusively found in the oxidation state +3, and is highly influenced by pH, with the optimal coordination conditions situated between pH 3 and 5, since a more acidic environment may inhibit the complex formation due to protonation of donor atoms, and a neutral or basic environment causes unreactive hydroxides to form. The constructs described in this study were prepared and radiolabelled with $^{68}GaCl_3$ following a standard procedure.[32] Briefly, to a dried aliquot of $^{68}GaCl_3$ was added a sample of NRs in 0.2 M sodium acetate solution and the reaction mixture was heated to 90 °C for 15 minutes, whilst monitoring by radio-thin layer chromatography (radio-TLC). In accordance with our previous results, the macrocyclic chelator was not required for the radiochemical incorporation of gallium-68 and quantitative radiolabelling was achieved in a 15 minute reaction time.[32] In order to simulate conditions of possible gallium(III) ion release *in vivo*, two assays were performed, see Fig. 5. Firstly, the radiolabelled constructs were incubated in human serum. All three constructs (**1–3**) showed high stability (>95%) after 3 hours at 37 °C, a reasonable time point considering the short half-life of gallium-68 (68 min). As gallium(III) has a similar atomic radius to iron(II), the primary mechanism for gallium(III) bioprocessing *in vivo* is *via* iron ion pathways, such as complexation with apo-trasnferrin in blood plasma.[45] In order to probe this property, the radiolabelled constructs (**1–3**) were incubated with an excess of apo-transferrin (0.5 mg) at 37 °C. Again, after 3 hours >95% of gallium-68 remained attached to the constructs, with no significant difference observed between differently coated NRs in either assay.

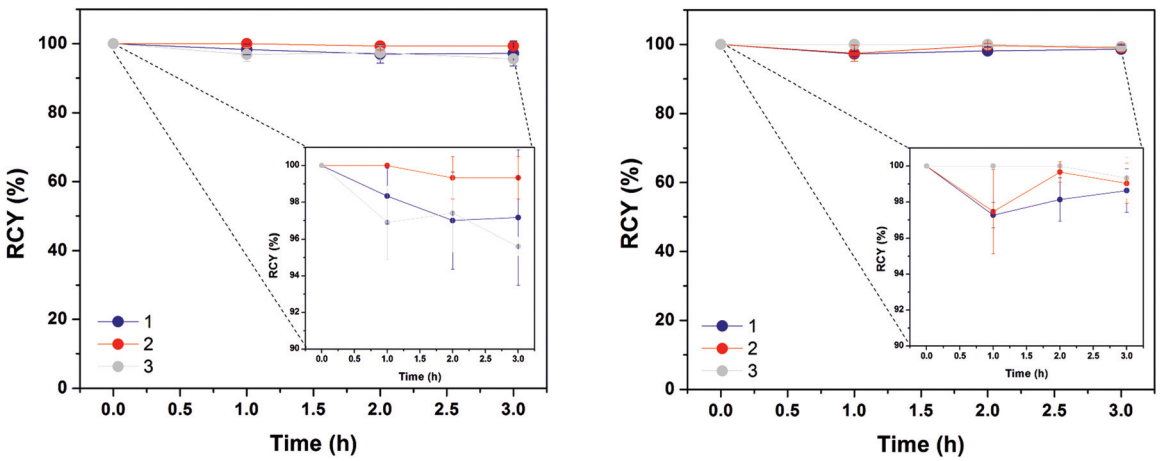

Fig. 5 Radiochemical stability of gallium-68 radiolabelled **1–3** in human serum (left) and apo-transferrin (right) over 3 hours, measured *via* radio-TLC.

Importantly, the ^{68}Ga radiolabelling results indicate that a bifunctional chelating agent is not required for rapid radiolabelling or to stably attach the metal ion *in vitro*, as demonstrated in chelator competition assays, with **3** showing analogous labelling stability to **1** and **2**. Experiments on comparable non-PEG silica coatings using triethoxy(ethyl)silane (data not shown) yielded equivalent radiochemical results, indicating that the effect is not solely a property of the PEG chains. Spectroscopic analysis of non-radioactive $^{69/71}$Ga isotope analogues failed to provide data on the existence of Ga–O–Si or Ga–O bonds as the peaks were masked by the intense Fe–O–Si and Fe–O peaks. Due to the polymeric nature of the surface coating and the high density, determined to be 37% w/w or 5.62 ligands per nm^2 of iron oxide for **3** (see Fig. S4†),[46] we assume that the attachment of gallium(III) to the core is unlikely. In order to assess the hypothesis of the formation of Ga–O–Si bonds, we attempted the ^{68}Ga radiochemistry at a lower pH, which would cause siloxy protonation and hence would not be able to react with the gallium(III). Reactions performed at pH 2 with **3** using the same temperature and reaction time yielded only 4.4% ± 0.9 (n = 3) RCY. Also, by modifying the pH of the same reactions back up to 5 and heating again for 15 minutes, the RCY increased to 96.7% ± 1.5 (n = 3), supporting this hypothesis.

2.4. *In vivo* imaging biodistribution and stability

All three radiolabelled NRs demonstrate comparable *in vitro* stability. The most interesting construct is **3** due to its lack of a chelator moiety. Thus, PET-CT and MR imaging studies were carried out in mice using gallium-68 labelled **3** to assess the co-localisation of PET and MRI signals and evaluate the *in vivo* stability of the construct.

Iron oxide nanoparticles of a similar size to ones used in this study are quickly taken up by the reticuloendothelial system (RES) and accumulate in the liver and spleen.[12,37,47] PET scanning revealed that the ^{68}Ga-**3** construct rapidly (<5 min) accumulated in the liver (Fig. 6). Some limited uptake in the lung was noted in some scans; this has been observed previously with iron oxide nanoparticles and has been attributed to possible embolisation caused by post-injection aggregation.[48,49] After the PET-CT study the mouse was transferred to the MR scanner and both T_1 and T_2 MR images were acquired (see Fig. 6 and S6†). As expected the liver T_1 signal was not significantly affected by the ^{68}Ga-**3** construct. Whereas T_2 weighted images revealed hypointense liver signal intensity, indicating localisation of the iron oxide NRs in the liver.

As a comparison, $^{68}Ga^{3+}$ was administered as gallium(III) citrate and its biodistributon assessed in order to observe the biodistribution that may occur if the ^{68}Ga were released from

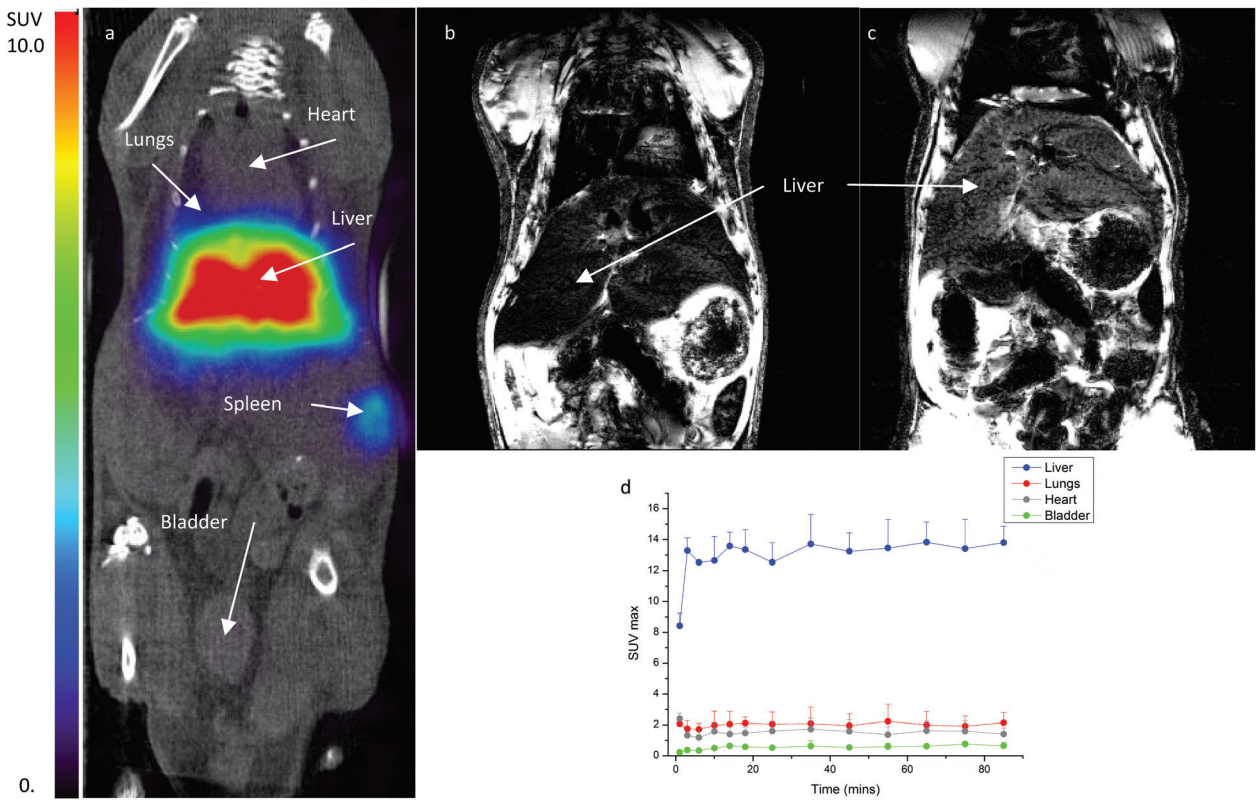

Fig. 6 *In vivo* mouse images of (a) 10 MBq/50 μg Fe of ^{68}Ga-**3**, fused PET-CT coronal slice image showing areas of main organ uptake at 80–90 minutes post-injection, (b) 10 MBq/50 μg Fe ^{68}Ga-**3**, T_2 weighted MR image at 90 minutes post-injection, (c) control mouse without nanoparticle administration, T_2 weighted MR image at 90 minutes post-injection and (d) time-activity-curve for major organs from PET image after administration of 10 MBq/50 μg Fe of ^{68}Ga-**3**.

the nanorod *in vivo*. PET scans show that the 'free' $^{68}Ga^{3+}$ is distributed more widely throughout multiple organs and is cleared much more slowly from the blood pool, see Fig. S5.† A significantly lower amount of radioactivity is noted in the liver, which is expected due to ^{68}Ga coordination to transferrin.

The presence of ^{68}Ga on the nanoparticle was also confirmed by *ex vivo* analysis, see Fig. S7.† After sacrifice (90 min post-injection), the liver was harvested and processed to separate the nanoparticles from the cell pellet, after which radio-TLC was used to determine if the radioactivity was still attached to the nanoparticle. As a comparison, the same experiment was carried out after independent administration of ^{68}Ga-citrate and ^{68}Ga-transferrin. It can be seen that after administration of $^{68}Ga^{3+}$ or ^{68}Ga-transferrin, the majority of the radioactivity is attached to transferrin. When ^{68}Ga-**3** is administered, >90% of the radioactivity is still attached to the nanorods even after analysis 90 min post-injection, which is a relatively late *in vivo* time point for gallium-68 imaging given its short half-life.

Debate is ongoing as to the best design parameters and applications for combined PET/MR imaging agents.[50] Iron–oxide nanoparticles of this size localise in the liver *via* phagocytosis into the Kupffer cells and malignant liver legions often lack normal Kupffer cells and remain "bright" in an MRI scan upon SPION administration.[51,52] However, the lower MRI sensitivity means that differentiation between regions with and without SPION may be challenging and may limit widespread clinical utility. Clinical utility could be increased by using PET radioisotope labelled SPIONs such as those developed in this study due to the increased sensitivity of PET and subsequent clarity of low uptake regions.

3 Conclusion

In this study, we have demonstrated that the positron emitting radioisotope ^{68}Ga can be used to radiolabel silica coated iron–oxide nanorods *via* surface interactions in the absence of a bifunctional chelating agent. Studies of ^{68}Ga-**3** (NRs coated with 100% PEG) confirm that the construct is stable *in vivo* and demonstrate its applicability as a PET/MR multimodal imaging agent. This is particularly interesting, because coated NRs can be easily obtained in one step from commercial materials, removing challenging and complex organic synthesis steps. Thus, this study establishes a novel straightforward method for the preparation of PET/MR multimodal imaging agents which have the potential to combine the high sensitivity of PET with MR contrast for malignant liver lesion imaging and also offer the potential for facile surface labelling methods that can be applied to currently licensed iron oxide MRI contrast agents for clinical use. This would facilitate more rapid progress through patient trials to regulatory approval.

4 Experimental

4.1. Materials and methods

Tri-*tert*-butyl-2,2′,2″-(10-(2-hydroxy-3-(3-(triethoxysilyl)propoxy)-propyl)-1,4,7,10-tetraazacyclododecane-1,4,7-triyl)triacetate (Siloxane-DO3A) and uncoated iron oxide nanorods were synthesised following literature proceedures.[32] 2-Methoxy-(polyethyleneoxy) propyltrimethoxysilane (Siloxane-PEG, M_W 1120–1250) was purchased from Gelest Inc. (Germany). All other chemicals were purchased from Sigma Aldrich, Acros or Alfa Aesar. External rare earth magnet (N42, NdFeB, 30 × 30 × 40 mm) was purchased from MagnetExpert Ltd. Transition Emission Microscopy (TEM) was performed on air dried suitable diluted samples deposited on a carbon-coated copper grid. Images were obtained using a Gatan US4000 digital camera (Gatan UK, Abingdon, Oxford) mounted onto a JEOL 2010 transmission electron microscope (Jeol UK) running at 200 kV. FTIR spectra were collected using a Fourier transform infra-red spectrometer manufactured by Perkin Elmer (model Spectrum RXI). Nanoparticle tracking analysis (NTA) was carried out with a LM10-HS microscope from NanoSight® using a 75 mW laser at 532 nm (green). Zeta potential was measured with Zeta Nanosizer (Malvern Instruments, ZEN3600, UK) at 25 °C, the conversion of the electrophoretic mobility (μ) into zeta potential (ζ) was performed using the Smoluchowski equation. Elemental analysis for carbon, hydrogen and nitrogen was carried out using a CHN analyser EA1108 (Carlo Erba). Inductively Coupled Optical Emission Spectroscopy (ICP-OES) analysis was performed using a Perkin Elmer Optima 5300 DV. All the samples were in solid state, digested with aqua regia in glass sample vials on a hotplate. Calibration standards were prepared at 1 and 10 ppm from 1000 ppm concentrates of iron and silicon which were purchased from Romil UK. Gallium-68 was eluted from a 740 MBq $^{68}Ge/^{68}Ga$ generator (iThemba LABS/IDB Holland) and prepared for synthesis following literature methods.[32] Radio-TLC analyses were carried out using either a 1480 Wizard 3″ Gamma Counter or Lablogic Scan-Ram, equipped with a NaI detector at a speed of 10 mm min^{-1}. Data were recorded using Lablogic Laura (version 4.1.7.70) after developing silica plates (TLC-SG, Merck KGaA) in aqueous 0.1 M citric acid to separate ^{68}Ga-NRs (R_f = 0), ^{68}Ga-transferrin (R_f = 0.5) and $^{68}Ga^{3+}$ (R_f = 1).

4.2. Synthesis of coated iron–oxide nanorods

General procedure for coating nanorods with siloxanes: freshly prepared nanorods were coated with siloxane-DO3A and 2-methoxy(polyethyleneoxy) propyltrimethoxysilane (Siloxane-PEG) in different ratios. In each reaction, bare NRs (0.3 g, 1.3 mmol) were suspended under nitrogen in 60% ethanol (100 ml) by extensive sonication. Ammonium hydroxide (20 ml, 35%) was added drop-wise and the solution was stirred for 30 min. The designated ratio of siloxane-DO3A and siloxane-PEG (total 0.34 mmol) was dissolved in ethanol (10 ml) and added over 10 min, the reaction was then stirred for 48 hours at room temperature. The solid precipitate formed was attracted to the bottom of the flask using an external rare earth magnet and the clear aqueous supernatant liquid was decanted. The washing and decanting procedure was repeated with 60% ethanol (2 × 100 ml), ethanol (2 × 100 ml), methanol (2 × 100 ml) and diethyl ether (100 ml) and dried. The crude sample was re-suspended in water (20 ml) filtered through a

5 μm filter followed by a 0.45 μm filter (Merck®) and dried under high vacuum to give coated NRs as a black/brown powder. Nanorods functionalised with 100% siloxane-DO3A or with 50% siloxane-DO3A were suspended in DCM (20 ml), TFA (2 ml) was added and the reaction was shaken at room temperature for 24 hours. The solid precipitate was attracted to the bottom of the flask using an external rare earth magnet and the clear aqueous supernatant liquid was decanted. The washing and decanting procedure was repeated with ethanol (2 × 20 ml), methanol (20 ml) and diethyl ether (100 ml) and dried. As previously, the crude sample was re-suspended in water (20 ml) filtered through a 5 μm filter followed by a 0.45 μm filter (Merck®) and dried under high vacuum to give coated NRs as a black/brown powder. (**1** = 124 mg, **2** = 154 mg, **3** = 97 mg).

4.3. MRI relaxivity studies

Relaxivity measurements were carried out on a clinical 3.0 T Discovery MR750 General Electric scanner. Longitudinal (T_1) and transverse (T_2) relaxation times were determined at a range of iron concentrations: 1, 0.5, 0.25 and 0.125 mM in water. A linear plot of concentration *versus* 1/relaxation time gives r_1 and r_2 as the plot gradient.

4.4. PET/CT image acquisition and image analysis

CD1 nude female mice (Charles River, UK) were anaesthetised with 1–2% Isoflurane, the tail vein was catheterised and they were placed in the Minerve Small-Animal Imaging Cell (Minerve, France) and transferred to the SuperArgus 2R preclinical PET/CT scanner (Sedecal, Spain). At the start of the PET acquisition, animals were injected with ~10 MBq, 50 μg Fe of ^{68}Ga-**3** intravenously(IV) *via* the tail vein and a 90-minute whole-body imaging sequence acquired (2 bed positions of 2 × 60 s, 4 × 120 s and 7 × 300 s). CT images were acquired *via* 360 projections/8 shots at a tube voltage of 45 kV and current of 140 μA. Respiration and temperature were monitored throughout using the SA Instruments 1025 T monitoring system (SA Instruments, CA, USA). All procedures were approved by the University of Hull Animal Welfare Ethical Review Body (AWERB) and carried out in accordance with the Animals in Scientific Procedures Act 1986 and the UKCCCR Guideline 2010[53] by approved protocols following institutional guidelines (Home Office Project License number 60/4549 held by Dr. Cawthorne).

4.5. MR image acquisition

Magnetic resonance imaging was performed on a wide bore vertical 11.7 T MR scanner (Bruker, Germany). With a 4 cm vertical field of view with slide thickness' of 1.0 mm and interslice distances of 1.5 mm. T_1 images were acquired using a RARE inverse recovery sequence in which TE = 7.5 ms, TR = 3500 ms, flip angle = 180°, SW = 79 365.1 Hz. T_2 images were acquired using a T_2 weighted FLASH sequence in which TE = 6.9 ms, TR = 350 ms, flip angle = 30°, SW = 50 505.1 Hz.

4.6. ^{68}Ga-3 *in vivo* liver stability

^{68}Ga-transferrin synthesis. Processed and dried $^{68}GaCl_3$ was added to apo-transferrin (0.5 mg) in water (200 μl) and incubated at 37 °C for 30 minutes. Radio-TLC indicated the synthesis of ^{68}Ga-transferrin in >95% radiochemical purity.

***Ex vivo* liver processing.** The liver was removed after sacrifice and ground in liquid nitrogen. The liver samples (*ca.* 80 mg) were added to lysis buffer (New England Biolabs (UK)) (10× w/w), sonicated for 10 minutes then centrifuged at 20 000 RPM for 10 minutes. The supernatant was separated from the cell pellet. Radio-TLC was carried out on the supernatant to determine gallium attachment.

Acknowledgements

The authors would like to thank Ann Lowry for carrying out TEM experiments, Bob Knight for performing the ICP-OES measurements and Carol Kennedy for carrying out CHN analyses. We gratefully acknowledge the Daisy Appeal Charity for funding (Grant: DAhul0211) and the University of Hull for support of the PET Research Centre. NB would like to thank the Saudi Arabian Cultural Bureau for a Saudi Government Scholarship (S2042). The research leading to these results has received funding (AK) from the People Programme (Marie Curie Actions) of the European Union's Seventh Framework Programme FP7/2007–2013/under REA grant agreement No. 607868 (iTERM). This work was supported by STSM Grants from MPNS EU COST Action TD1007 "Bimodal PET-MRI molecular imaging technologies and applications for *in vivo* monitoring of disease and biological processes". MDP and PG express their thanks to Yorkshire Cancer Research for the charity's continuing support. We thank Dr Assem Allam for his generous donation and ongoing support to the PET Research Centre at the University of Hull.

Notes and references

1 P. W. Miller, N. J. Long, R. Vilar and A. D. Gee, *Angew. Chem., Int. Ed.*, 2008, **47**, 8998.
2 P. Blower, *Dalton Trans.*, 2006, 1705.
3 E. W. Price and C. Orvig, *Chem. Soc. Rev.*, 2014, **43**, 260.
4 R. R. Raylman, S. Majewski, S. Lemieux, S. S. Velan, B. Kross, V. Popov, M. F. Smith, A. G. Weisenberger and R. Wojcik, *Nucl. Instrum. Methods Phys. Res., Sect. A*, 2006, **569**, 306.
5 F. Gerstl, C. Windischberger, M. Mitterhauser, W. Wadsak, A. Holik, K. Kletter, E. Moser, S. Kasper and R. Lanzenberger, *NeuroImage*, 2008, **41**, 204.
6 X. Q. Yang, H. Hong, J. J. Grailer, I. J. Rowland, A. Javadi, S. A. Hurley, Y. L. Xiao, Y. A. Yang, Y. Zhang, R. Nickles, W. B. Cai, D. A. Steeber and S. Q. Gong, *Biomaterials*, 2011, **32**, 4151.
7 L. E. Jennings and N. J. Long, *Chem. Commun.*, 2009, 3511.
8 J.-s. Choi, J. C. Park, H. Nah, S. Woo, J. Oh, K. M. Kim, G. J. Cheon, Y. Chang, J. Yoo and J. Cheon, *Angew. Chem., Int. Ed.*, 2008, **47**, 6259.

9 L. Frullano, C. Catana, T. Benner, A. D. Sherry and P. Caravan, *Angew. Chem., Int. Ed.*, 2010, **49**, 2382.
10 M. Colombo, S. Carregal-Romero, M. F. Casula, L. Gutierrez, M. P. Morales, I. B. Bohm, J. T. Heverhagen, D. Prosperi and W. J. Parak, *Chem. Soc. Rev.*, 2012, **41**, 4306.
11 E. C. Cho, C. Glaus, J. Y. Chen, M. J. Welch and Y. N. Xia, *Trends Mol. Med.*, 2010, **16**, 561.
12 R. Qiao, C. Yang and M. Gao, *J. Mater. Chem.*, 2009, **19**, 6274.
13 J. W. M. Bulte and D. L. Kraitchman, *NMR Biomed.*, 2004, **17**, 484.
14 C. Sun, J. S. H. Lee and M. Zhang, *Adv. Drug Delivery Rev.*, 2008, **60**, 1252.
15 A. K. Gupta and M. Gupta, *Biomaterials*, 2005, **26**, 3995.
16 A. K. Gupta, R. R. Naregalkar, V. D. Vaidya and M. Gupta, *Nanomed.*, 2007, **2**, 23.
17 Y. X. J. Wang, S. M. Hussain and G. P. Krestin, *Eur. Radiol.*, 2001, **11**, 2319.
18 W.-W. Wang and J.-L. Yao, *Mater. Lett.*, 2010, **64**, 840.
19 A. F. Rebolledo, S. Laurent, M. Calero, A. Villanueva, M. Knobel, J. F. Marco and P. Tartaj, *ACS Nano*, 2010, **4**, 2095.
20 S. Nath, C. Kaittanis, V. Ramachandran, N. S. Dalal and J. M. Perez, *Chem. Mater.*, 2009, **21**, 1761.
21 P. Kolhar, A. C. Anselmo, V. Gupta, K. Pant, B. Prabhakarpandian, E. Ruoslahti and S. Mitragotri, *Proc. Natl. Acad. Sci. U. S. A.*, 2013, **110**, 10753.
22 B. P. Burke, G. S. Clemente and S. J. Archibald, *J. Labelled Compd. Radiopharm.*, 2014, **57**, 239.
23 M. D. Bartholomä, *Inorg. Chim. Acta*, 2012, **389**, 36.
24 J.-F. Morfin and E. Toth, *Inorg. Chem.*, 2011, **50**, 10371.
25 T. J. Wadas, E. H. Wong, G. R. Weisman and C. J. Anderson, *Chem. Rev.*, 2010, **110**, 2858.
26 R. E. Mewis and S. J. Archibald, *Coord. Chem. Rev.*, 2010, **254**, 1686.
27 E. Wong, P. Caravan, S. Liu, S. J. Rettig and C. Orvig, *Inorg. Chem.*, 1996, **35**, 715.
28 D. J. Berry, Y. Ma, J. R. Ballinger, R. Tavare, A. Koers, K. Sunassee, T. Zhou, S. Nawaz, G. E. D. Mullen, R. C. Hider and P. J. Blower, *Chem. Commun.*, 2011, **47**, 7068.
29 S. Liu and D. S. Edwards, *Bioconjugate Chem.*, 2001, **12**, 7.
30 B. P. Burke and S. J. Archibald, *Annu. Rep. Prog. Chem., Sect. A: Inorg. Chem.*, 2013, **109**, 232.
31 G. J. Stasiuk and N. J. Long, *Chem. Commun.*, 2013, **49**, 2732.
32 B. P. Burke, N. Baghdadi, G. S. Clemente, N. Camus, A. Guillou, A. E. Kownacka, J. Domarkas, Z. Halime, R. Tripier and S. J. Archibald, *Faraday Discuss.*, 2014, **175**, 59.
33 E. K. U. Larsen, T. Nielsen, T. Wittenborn, H. Birkedal, T. Vorup-Jensen, M. H. Jakobsen, L. Ostergaard, M. R. Horsman, F. Besenbacher, K. A. Howard and J. Kjems, *ACS Nano*, 2009, **3**, 1947.
34 M. Ma, Y. Zhan, Y. Shen, X. Xia, S. Zhang and Z. Liu, *J. Nanopart. Res.*, 2011, **13**, 3249.
35 M. Mahmoudi, S. Sant, B. Wang, S. Laurent and T. Sen, *Adv. Drug Delivery Rev.*, 2011, **63**, 24.
36 C. Nazli, T. I. Ergenc, Y. Yar, H. Y. Acar and S. Kizilel, *Int. J. Nanomed.*, 2012, **7**, 1903.
37 A.-C. Faure, S. Dufort, V. Josserand, P. Perriat, J.-L. Coll, S. Roux and O. Tillement, *Small*, 2009, **5**, 2565.
38 J. Moreau, E. Guillon, J. C. Pierrard, J. Rimbault, M. Port and M. Aplincourt, *Chem. – Eur. J.*, 2004, **10**, 5218.
39 C. M. Fisher, E. Fuller, B. P. Burke, V. Mogilireddy, S. J. A. Pope, A. E. Sparke, I. Dechamps-Olivier, C. Cadiou, F. Chuburu, S. Faulkner and S. J. Archibald, *Dalton Trans.*, 2014, **43**, 9567.
40 H. S. Choi, W. Liu, P. Misra, E. Tanaka, J. P. Zimmer, B. I. Ipe, M. G. Bawendi and J. V. Frangioni, *Nat. Biotechnol.*, 2007, **25**, 1165.
41 P. Bouziotis, D. Psimadas, T. Tsotakos, D. Stamopoulos and C. Tsoukalas, *Curr. Top. Med. Chem.*, 2012, **12**, 2694.
42 F. Ye, S. Laurent, A. Fornara, L. Astolfi, J. Qin, A. Roch, A. Martini, M. S. Toprak, R. N. Muller and M. Muhammed, *Contrast Media Mol. Imaging*, 2012, **7**, 460.
43 L. Josephson, J. Lewis, P. Jacobs, P. F. Hahn and D. D. Stark, *Magn. Reson. Imaging*, 1988, **6**, 647.
44 H. Duan, M. Kuang, X. Wang, Y. A. Wang, H. Mao and S. Nie, *J. Phys. Chem. C*, 2008, **112**, 8127.
45 W. R. Harris and V. L. Pecoraro, *Biochemistry*, 1983, **22**, 292.
46 Y. B. Sun, X. B. Ding, Z. H. Zheng, X. Cheng, X. H. Hu and Y. X. Peng, *Chem. Commun.*, 2006, **42**, 2765.
47 F. Alexis, E. Pridgen, L. K. Molnar and O. C. Farokhzad, *Mol. Pharm.*, 2008, **5**, 505.
48 E. Locatelli, L. Gil, L. L. Israel, L. Passoni, M. Naddaka, A. Pucci, T. Reese, V. Gomez-Vallejo, P. Milani, M. Matteoli, J. Llop, J. P. Lellouche and M. C. Franchini, *Int. J. Nanomed.*, 2012, **7**, 6021.
49 M. Jauregui-Osoro, P. A. Williamson, A. Glaria, K. Sunassee, P. Charoenphun, M. A. Green, G. E. D. Mullen and P. J. Blower, *Dalton Trans.*, 2011, **40**, 6226.
50 R. T. M. de Rosales, *J. Labelled Compd. Radiopharm.*, 2014, **57**, 298.
51 D.-M. Koh, *Cancer Imaging*, 2012, **12**, 363.
52 S. Maurea, P. P. Mainenti, A. Tambasco, M. Imbriaco, C. Mollica, E. Laccetti, L. Camera, R. Liuzzi and M. Salvatore, *Quant. Imaging Med. Surg.*, 2014, **4**, 181.
53 P. Workman, E. O. Aboagye, F. Balkwill, A. Balmain, G. Bruder, D. J. Chaplin, J. A. Double, J. Everitt, D. A. H. Farningham, M. J. Glennie, L. R. Kelland, V. Robinson, I. J. Stratford, G. M. Tozer, S. Watson, S. R. Wedge, S. A. Eccles, V. Navaratnam, S. Ryder and I. Natl Canc Res, *Br. J. Cancer*, 2010, **102**, 1555.